Mesenchymal Stem Cells Aggregate and Deliver Gold Nanoparticles to Tumors for Photothermal Therapy

Seokyung Kang,[†,□] Suk Ho Bhang,[‡,□] Sekyu Hwang,[∥] Jeong-Kee Yoon,[†] Jaejung Song,[⊥] Hyeon-Ki Jang,[§] Sungjee Kim,[∥,⊥] and Byung-Soo Kim*[,†,§,#]

[†]School of Chemical and Biological Engineering, [§]Interdisciplinary Program for Bioengineering, and [#]Bio-MAX Institute, Institute for Chemical Processes, Seoul National University, Seoul 151-742, Republic of Korea, [‡]School of Chemical Engineering, Sungkyunkwan University, Suwon 440-746, Republic of Korea, and [∥]School of Chemistry and [⊥]School of Interdisciplinary Bioscience and Bioengineering, Pohang University of Science & Technology (POSTECH), Pohang 790-784, Republic of Korea. [□]S. Kang and S. H. Bhang contributed equally to this work.

ABSTRACT Gold nanoparticles (AuNPs) have been extensively studied for photothermal cancer therapy because AuNPs can generate heat upon near-infrared irradiation. However, improving their tumor-targeting efficiency and optimizing the nanoparticle size for maximizing the photothermal effect remain challenging. We demonstrate that mesenchymal stem cells (MSCs) can aggregate pH-sensitive gold nanoparticles (PSAuNPs) in mildly acidic endosomes, target tumors, and be used for photothermal therapy. These aggregated structures had a higher cellular retention in comparison to pH-insensitive, control AuNPs (cAuNPs), which is important for the cell-based delivery process. PSAuNP-laden MSCs (MSC-PSAuNPs) injected intravenously to tumor-bearing mice show a 37-fold higher tumor-targeting efficiency (5.6% of the injected dose) and 8.3 °C higher heat generation compared to injections of cAuNPs after irradiation, which results in a significantly enhanced anticancer effect.

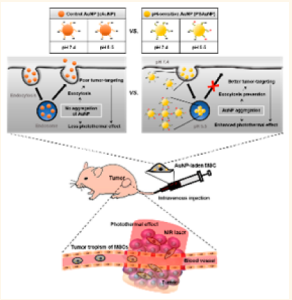

KEYWORDS: gold nanoparticles · mesenchymal stem cells · pH-sensitive · photothermal therapy · tumor tropism

Plasmonic photothermal therapy is a spatiotemporally controllable strategy for cancer treatment.[1] The localized heat is generated by photothermal agents that can convert light to heat. This can cause irreversible cell damage depending on the magnitude of the temperature and exposure time. Near-infrared (NIR) laser light is typically used to maximize the tissue penetration, as skin and tissues minimally absorb light at NIR wavelengths.[2] Conventional hyperthermia (43−48 °C) treatment increases the rate of biochemical reactions, which induces the generation of reactive oxygen species. This oxidative stress gradually leads to the destruction of plasma membranes, proteins, and nucleic acid.[3,4] For direct cell necrosis, long-term exposures (>60 min) to temperatures in this range are required.[4,5] On the other hand, temperatures above 48 °C instantaneously cause irreversible protein coagulation and DNA damage that lead to cell death even for short exposure times (4−6 min).[4] The advantages of photothermal therapy to eliminate tumor tissues are spatiotemporal controllability, minimal invasiveness, and independence of tumor type.[6]

Gold nanoparticles (AuNPs) have been intensively investigated as a photothermal agent for photothermal cancer therapy.[7−9] AuNPs efficiently generate heat by absorbing the extrinsic light energy at the plasmonic resonant wavelength. Previous studies have reported on efficient photothermal therapy using NIR-responsive gold nanostructures such as nanoshells,[10] nanorods,[11] and nanomatryoshkas.[12] Here, we used previously developed pH-sensitive AuNPs (PSAuNPs) that selectively aggregate under mild acidic conditions.[9] The PSAuNPs consist of ∼10 nm gold nanospheres, which can be easily synthesized in large scale,[13] and pH-susceptible surface ligands. Under mild acidic conditions, such as the pH in cellular acidic endosomes/lysosomes, the negatively charged surfaces of PSAuNPs are converted to positive and negative charges, which rapidly causes aggregation of the nanoparticles through electrostatic interactions. As the aggregation of AuNPs induces the absorption red-shift to the NIR region,

* Address correspondence to (B.-S. Kim) byungskim@snu.ac.kr.

Received for review April 14, 2015 and accepted September 8, 2015.

Published online September 08, 2015
10.1021/acsnano.5b02207

PSAuNP aggregates exhibit stronger photothermal effects upon NIR irradiation compared to unmodified AuNPs.[9] Although various gold nanostructures that can efficiently generate heat upon NIR laser irradiation have been developed, it still remains challenging to improve the tumor-targeting efficiency and intratumoral distribution of these nanostructures for effective photothermal treatment.

Tumor-tropic cells including macrophages[14−16] and neural stem cells (NSCs)[17] have been used as delivery vehicles that can transport nanoparticle to tumor tissues. Macrophages loaded with gold nanoshells migrated within glioma spheroids *in vitro* and generated heat upon laser irradiation.[14,15] Tumor-tropic properties of macrophages were demonstrated in a brain-tumor-bearing mouse model.[16] Gold-nanoshell-laden macrophages migrated into brain tumors by traversing the blood−brain barrier, meanwhile intratumoral injection of gold-nanorod-loaded NSCs improved the intratumoral distribution of the nanorods and consequently enhanced the photothermal therapeutic efficacy.[17] Here, we used tumor-tropic mesenchymal stem cells (MSCs) to aggregate and deliver AuNPs to tumors. Furthermore, MSCs can be easily isolated from patients and extensively expanded *in vitro*.[18] MSCs also exhibit minimal immunogenicity and even immunosuppressive property upon transplantation.[18,19] Therefore, AuNP-laden MSCs can serve as a stealth vehicle to deliver AuNPs to tumors, as they can avoid the surveillance of immune cells to safely arrive at the target tumor tissues.

In cell-mediated nanoparticle delivery systems, it is important to retain the loaded AuNPs within cells during their migration to the tumor tissues because nanoparticles can easily escape from cells through exocytosis.[20] This lowers the tumor-targeting efficiency of the nanoparticles. The endocytosis and exocytosis of nanoparticles depend on the size and shape of the nanoparticles.[20,21] Spherical-shaped PSAuNPs can be efficiently endocytosed into cells, and the formation of large-sized PSAuNP aggregates in cells can prevent their exocytosis,[20,21] consequently enhancing cellular retention. In this study, we hypothesized that MSCs loaded with PSAuNPs (MSC-PSAuNPs) would enhance the tumor-targeting efficiency and the plasmonic photothermal effect of AuNPs by inducing the aggregation of AuNPs within the MSCs and reducing AuNP exocytosis. First, we investigated whether high loading of PSAuNPs in MSCs could be obtained by efficiently reducing the exocytosis of PSAuNPs *via* PSAuNP aggregation in the MSCs (see mechanism in Figure 1). Then, we investigated whether the *in vitro* photothermal capability of the PSAuNP aggregates in MSCs, which were larger in size than pH-insensitive, control AuNPs (cAuNPs) in MSCs, was improved. Following intravenous injection of MSC-PSAuNPs into tumor-bearing mice, we demonstrated the high tumor-targeting efficiency of the MSC-PSAuNPs *via* imaging and investigated the biodistributions of AuNPs in the tumor tissues and distant organs. The enhanced photothermal therapeutic efficiency of the MSC-PSAuNP was demonstrated by observing the prognosis for 21 days and performing gene expression and histological analysis.

RESULTS AND DISCUSSION

Characterization of PSAuNPs. PSAuNPs were prepared using the method described in our previous report.[9] The pH-sensitive aggregation of PSAuNPs was examined in buffer solutions under pH 7.4 or 5.5. We observed the surface plasmon resonance of the AuNPs by monitoring the absorption over time. The cAuNPs exhibited no noticeable absorption change in both the pH 5.5 and pH 7.4 buffer environments (Figure 2a). In contrast, the PSAuNPs in the pH 5.5 environment exhibited a continuous absorption red-shift and broadening over time, although in the pH 7.4 environment they exhibited negligible absorption change (Figure 2a). These results indicate a pH-sensitive aggregation of the PSAuNPs, as the broadening red-shifted absorption is attributed to the coupled plasmons between closely located AuNPs.[9] The zeta-potential and the hydrodynamic size of the AuNPs were measured over time in the pH 5.5 and pH 7.4 environments. Although the zeta-potential of the cAuNPs was −30 mV under both pH conditions, the PSAuNPs in the pH 5.5 exhibited significant changes in the zeta-potential from −30 mV to −9 mV (Figure 2b). This indicates that the surface charge of the PSAuNPs was partially converted from negative to positive under mild acidic conditions. The hydrodynamic size changes coincided with the zeta-potential. The cAuNPs retained their initial hydrodynamic size (14 nm) throughout the period (Figure 2c). In contrast, the PSAuNPs in pH 5.5 exhibited a rapid increase in hydrodynamic size from 14 nm to 90 nm within 30 min, whereas there was no noticeable change in pH 7.4 (Figure 2c). The transmission electron microscopy (TEM) analysis further confirmed the aggregation of PSAuNPs under acidic conditions. In the pH 5.5 environment, the PSAuNPs clustered over time, whereas no noticeable size change was observed for the cAuNPs (Figure 2d). Taken together, these results demonstrate that the PSAuNPs are indeed pH-sensitive.

To compare the properties of PSAuNPs and cAuNPs at the cellular level, PSAuNPs or cAuNPs were added to MSC culture. The TEM analysis revealed PSAuNP aggregates that were >200 nm in diameter within the intracellular vesicles (Figure 2e, Supporting Information Figure S1). The pH-sensitive aggregation property of the PSAuNPs likely led to the formation of PSAuNP clusters in the acidic endosomes of the MSCs. Next, the cellular uptake of the AuNPs was quantitatively evaluated using ICP-AES after incubating the MSCs with the same concentration of PSAuNPs or cAuNPs for 24 h. The MSCs treated with PSAuNPs exhibited a 4-fold higher accumulation than those treated with cAuNPs

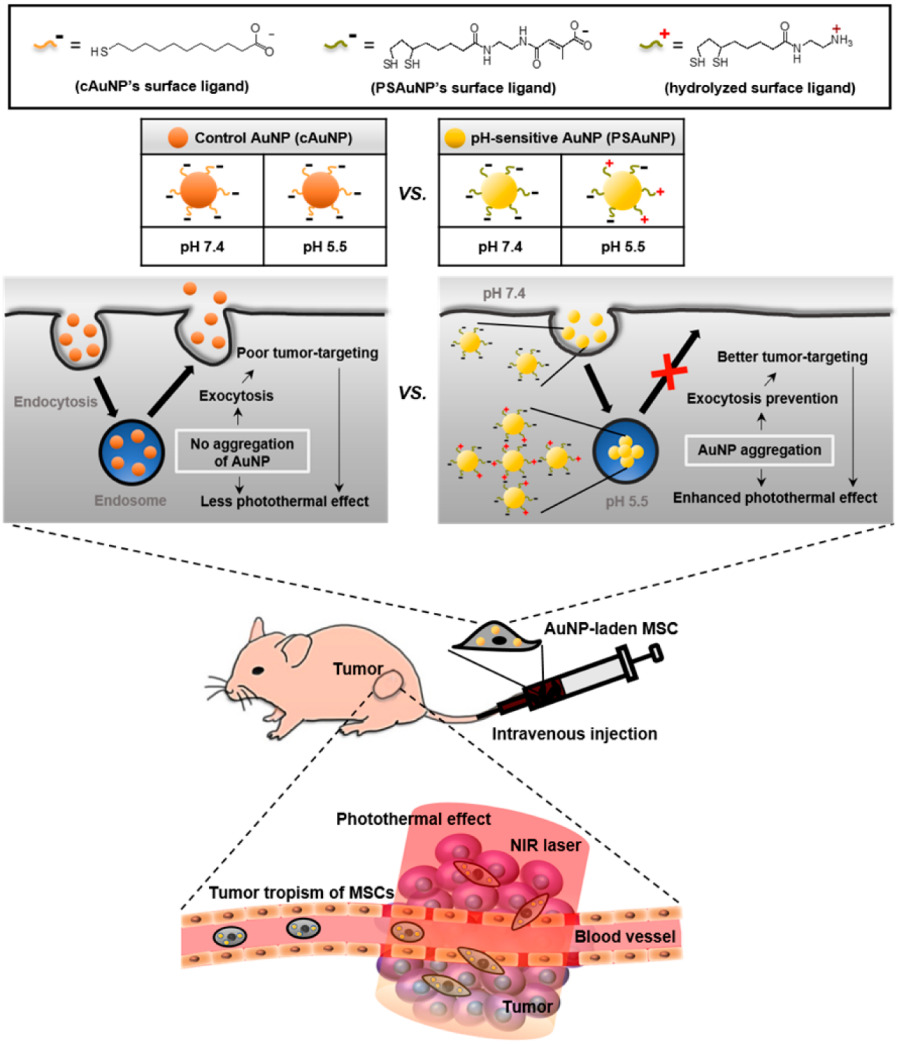

Figure 1. Schematic illustration of the working mechanisms of the improved tumor-targeting efficiency and photothermal effect of the AuNPs by employing pH-sensitive AuNP-laden mesenchymal stem cells (MSC-PSAuNPs). Unlike cAuNPs, PSAuNPs change their surface charge from negative charge to a mixture of negative and positive charges because some of the citraconic amide is hydrolyzed at a mild acidic condition. This partial hydrolysis of the PSAuNPs' surface ligands causes AuNP aggregation through electrostatic interactions. The AuNPs can be taken up by MSCs and delivered to the target tumor region *via* the tumor-tropic properties of MSCs. pH-insensitive cAuNPs are easily exocytosed from MSCs, which results in low tumor-targeting efficiency, and induce poor photothermal effects due to their small size and low tumor-targeting efficiency. In contrast, the cancer treatment strategy using MSC-PSAuNPs can enhance the anticancer therapeutic effects, as the PSAuNPs cluster together in acidic endosomes in the MSCs, which enhances the tumor-targeting efficiency of AuNPs *via* preventing exocytosis and increases the photothermal effect *via* the stronger resonant absorption.

(Figure 2f). A possible explanation for the increased content of AuNPs in the MSCs is the suppression of AuNP exocytosis. To examine the dynamics of AuNP exocytosis, the MSCs were cultured with PSAuNPs or cAuNPs for 24 h and washed three times to remove the noninternalized AuNPs. After replenishing the culture dish with fresh medium, the quantity of AuNPs in the MSCs was determined *via* ICP-AES at various culture time points (Figure 2g). We calculated the fraction of exocytosed AuNPs (F_{exo}) using the previously described equation:[20]

$$F_{exo} = \frac{N_{out}}{N_0}$$

where N_{out} is the quantity of AuNPs exocytosed from the MSCs at time t and N_0 is the initial quantity of AuNPs contained in the MSCs. Interestingly, a lower fraction of the PSAuNPs was exocytosed and at a slower rate compared to the cAuNPs (Figure 2g). At 72 h, the exocytosed fraction of the PSAuNPs (29%) was only half of that of the cAuNPs (60%). From the exocytosis kinetics, we inferred the half-life of the AuNPs, which was defined as the time taken to reach half of the fraction of exocytosed AuNPs at steady state.[20] The half-life values of the cAuNPs and PSAuNPs were 0.58 and 1.90 h, respectively. This result confirmed that the exocytosis rate of the PSAuNPs was much slower than that of the cAuNPs. Previous studies have demonstrated that both endocytosis and exocytosis of nanoparticles occur in a size-dependent manner.[20,21] Nanoparticles with diameters smaller than 100 nm

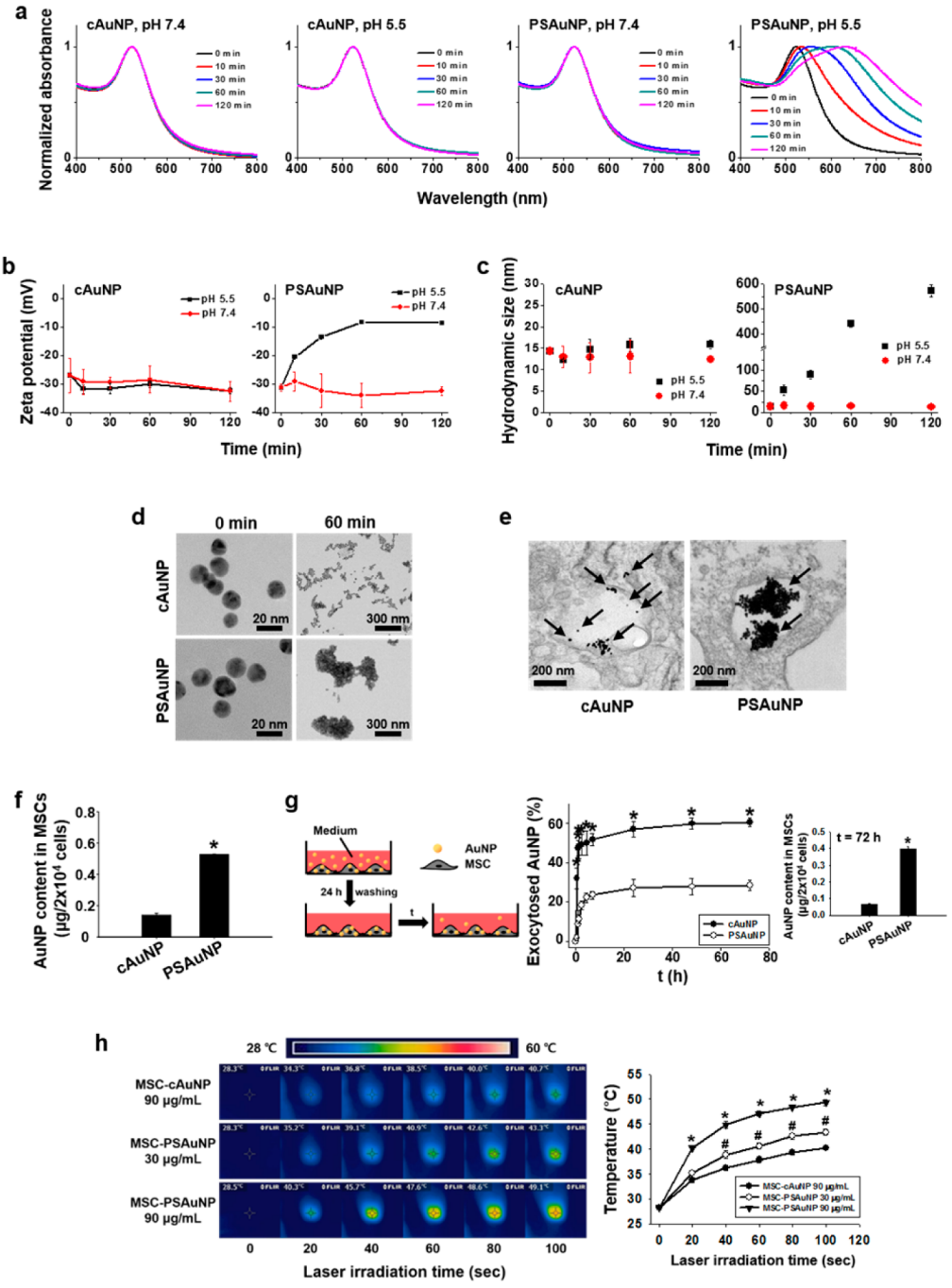

Figure 2. pH-dependent aggregation, exocytosis, and photothermal properties of the PSAuNPs in the MSCs. (a) Time evolution of absorption at pH 7.4 and pH 5.5 for cAuNPs and PSAuNPs. (b) Zeta-potential and (c) hydrodynamic size of the cAuNPs (left) and PSAuNPs (right) at pH 5.5 and pH 7.4. (d) TEM images of the cAuNPs and the PSAuNPs at pH 5.5 for various elapsed times. (e) TEM images showing the intracellular localization of AuNPs (arrows) after incubating the MSCs with the same concentration of cAuNPs or PSAuNPs for 24 h. Scale bars = 200 nm. (f) Intracellular amounts of AuNPs after incubating the MSCs with the same concentration (100 μg/mL) of cAuNPs or PSAuNPs for 24 h, as evaluated *via* ICP-AES ($n = 4$). *$p < 0.05$. (g) Time profiles of AuNP exocytosis ($n = 4$) and the intracellular amounts of AuNPs in the MSCs at $t = 72$ h ($n = 4$). The MSCs were cultured with the same concentration of PSAuNPs or cAuNPs for 24 h and then washed to eliminate the noninternalized AuNPs. After replenishing the culture dish with fresh medium, the amount of AuNPs in the cells was determined *via* ICP-AES over time to evaluate the exocytosed AuNPs at various time points (t). *$p < 0.05$. (h) Temperature profiles of the AuNP-laden MSCs during the laser irradiations ($n = 5$). *$p < 0.05$ *versus* any group, #$p < 0.05$ *versus* MSC-cAuNP 90 μg/mL group.

are not only more easily taken up by cells[21] but also more easily released from the cells.[20] The PSAuNPs exhibit ambivalent characteristics, which can lead to effective intracellular accumulation of AuNPs. Once the PSAuNPs (14 nm in size) at physiological pH are efficiently endocytosed, the PSAuNPs aggregates (>100 nm in size) are formed in acidic endosomes and poorly exocytosed.

The *in vitro* photothermal effect of the PSAuNP-laden MSCs was evaluated *via* a real-time infrared thermal imaging system during 660 nm laser irradiation at a power density of 0.5 W/cm^2 (Figure 2h). The temperature profiles of the MSCs following treatment with various concentrations of PSAuNP (30 or 90 μg/mL) or cAuNP (90 μg/mL) were observed for 100 s of laser irradiation. The photothermal effect of the AuNPs depends on the size and amount of AuNPs.[7,22,23] The resonant absorption properties of AuNPs induce heat generation upon laser irradiation.[24] As the diameter of AuNPs increases, the surface plasmon absorption is red-shifted toward the NIR region (Figure 2a). Therefore, with NIR laser irradiation, PSAuNP aggregates with larger diameters yield higher light-to-heat conversion than AuNPs with smaller diameters. The temperatures of the MSCs treated with the same concentration (90 μg/mL) of PSAuNPs and cAuNPs increased to 49.3 and 40.3 °C, respectively, after 100 s of irradiation (Figure 2h). The higher temperature in the MSC-PSAuNP 90 μg/mL group is attributed to the larger intracellular amount and size of the PSAuNPs. In addition, the MSC-PSAuNP 30 μg/mL group exhibited a higher temperature profile compared to the MSC-cAuNP 90 μg/mL group (Figure 2h).

Optimizing the PSAuNP Dose and Multiple Treatments. To maximize the quantity of PSAuNPs loaded in the MSCs, the PSAuNP dose and the PSAuNP treatment method must be optimized. The MSCs were incubated with various concentrations of PSAuNPs for 24 h. The cell viability was then evaluated using a cell counting kit-8 (CCK-8). Compared to the no-treatment group, the MSCs treated with 500 μg/mL PSAuNPs exhibited a significantly reduced cell viability (Figure 3a). However, 100 μg/mL PSAuNPs did not cause cytotoxicity, meanwhile the MSCs treated with 500 μg/mL cAuNPs did not exhibit cytotoxicity (Supporting Information Figure S2), which is likely due to cellular uptake of much lower amounts of cAuNPs compared to PSAuNPs (Figure 2f). A previous study has demonstrated that the negatively charged AuNPs, such as cAuNPs and PSAuNPs, can cause a dose-dependent cytotoxicity.[25] When a large amount of the negatively charged AuNPs are internalized into cells, the stressed mitochondria increase the intracellular amount of calcium ions.[25] Consequently, the cells treated with a large amount of the negatively charged AuNPs undergo calcium-evoked apoptosis.

Next, we investigated whether multiple treatments of MSCs with PSAuNPs increase the intracellular loading of PSAuNPs *in vitro*. In previous studies, cells have been subjected to only a single treatment of nanoparticles for cellular uptake.[14,26,27] MSCs were incubated with PSAuNPs for 2 days and then replenished with fresh medium containing new PSAuNPs. This procedure was carried out three times. The cell viability and apoptotic activity were assessed using live/dead imaging, Western blotting, quantitative real-time PCR (qRT-PCR), and immunocytochemical staining. The live/dead cell staining indicated that the three consecutive treatments with 100 μg/mL PSAuNPs caused cytotoxicity (Figure 3b). The Western blot analysis for a pro-apoptotic marker (caspase-3) and a proliferating cell nuclear antigen (PCNA) also demonstrated that the three consecutive treatments with 100 μg/mL PSAuNPs induced apoptotic activity and decreased the proliferating capability (Figure 3c). Furthermore, the MSCs treated with 100 μg/mL PSAuNPs three times exhibited increased mRNA expression of p53, a pro-apoptotic marker, and decreased expression of Bcl-2, an anti-apoptotic marker, compared to the other groups (Figure 3d). The number of caspase-3-positive cells was significantly increased in the 100 μg/mL PSAuNP $\times$ 3 group compared to the 50 μg/mL PSAuNP $\times$ 3 group (Figure 3e). These analyses confirmed that 50 μg/mL of PSAuNPs is a suitable concentration for the three repeated treatments because cell viability, proliferation, and apoptosis of the 50 μg/mL PSAuNP $\times$ 3 group were not significantly different compared to the no-treatment group (Figure 3b–e), meanwhile the three consecutive treatments with 50 μg/mL cAuNPs also did not cause cytotoxicity, but the 100 μg/mL cAuNP $\times$ 3 group exhibited a significantly reduced cell viability according to the CCK-8 (Supporting Information Figure S2).

Multiple treatments of MSCs with PSAuNPs increased intracellular loading of the PSAuNPs *in vitro*. The TEM analysis revealed that the intracellular amount of PSAuNP aggregates was increased in the MSC-PSAuNP 50 μg/mL $\times$ 3 group compared to the MSC-PSAuNP 150 μg/mL $\times$ 1 group (Figure 3f). The ICP-AES analysis for quantifying the intracellular PSAuNP content indicated that the MSC-PSAuNP 50 μg/mL $\times$ 3 group corresponded to 14.8-fold and 6.0-fold higher intracellular contents of PSAuNPs compared to the MSC-PSAuNP 50 μg/mL $\times$ 1 group and the MSC-PSAuNP 150 μg/mL $\times$ 1 group, respectively (Figure 3g). The PSAuNP content in cells in the 150 μg/mL PSAuNP treatment group was much smaller than that in the 50 μg/mL PSAuNP $\times$ 3 group (Figure 3g). This was likely due to the higher toxicity of the 150 μg/mL PSAuNP treatment compared to that of the 50 μg/mL PSAuNP $\times$ 3 treatment (Figure 3c–e). For the determination of intracellular AuNP contents, cells were washed with PBS three times. In this procedure, a large amount of PSAuNPs was likely washed out from the dead cells in the 150 μg/mL PSAuNP treatment group, which contains more dead cells than the 50 μg/mL PSAuNP $\times$ 3 treatment group. As shown in the TEM images (Figure 3f), the PSAuNPs in the MSCs were located in vesicles, which indicates that the PSAuNPs were internalized primarily *via* endocytosis.[28] In this pathway of cellular uptake, specific regions of the plasma membrane wrap around the PSAuNPs and then detach to form internalized vesicles. As the surface area and the recovery time of the plasma membrane are

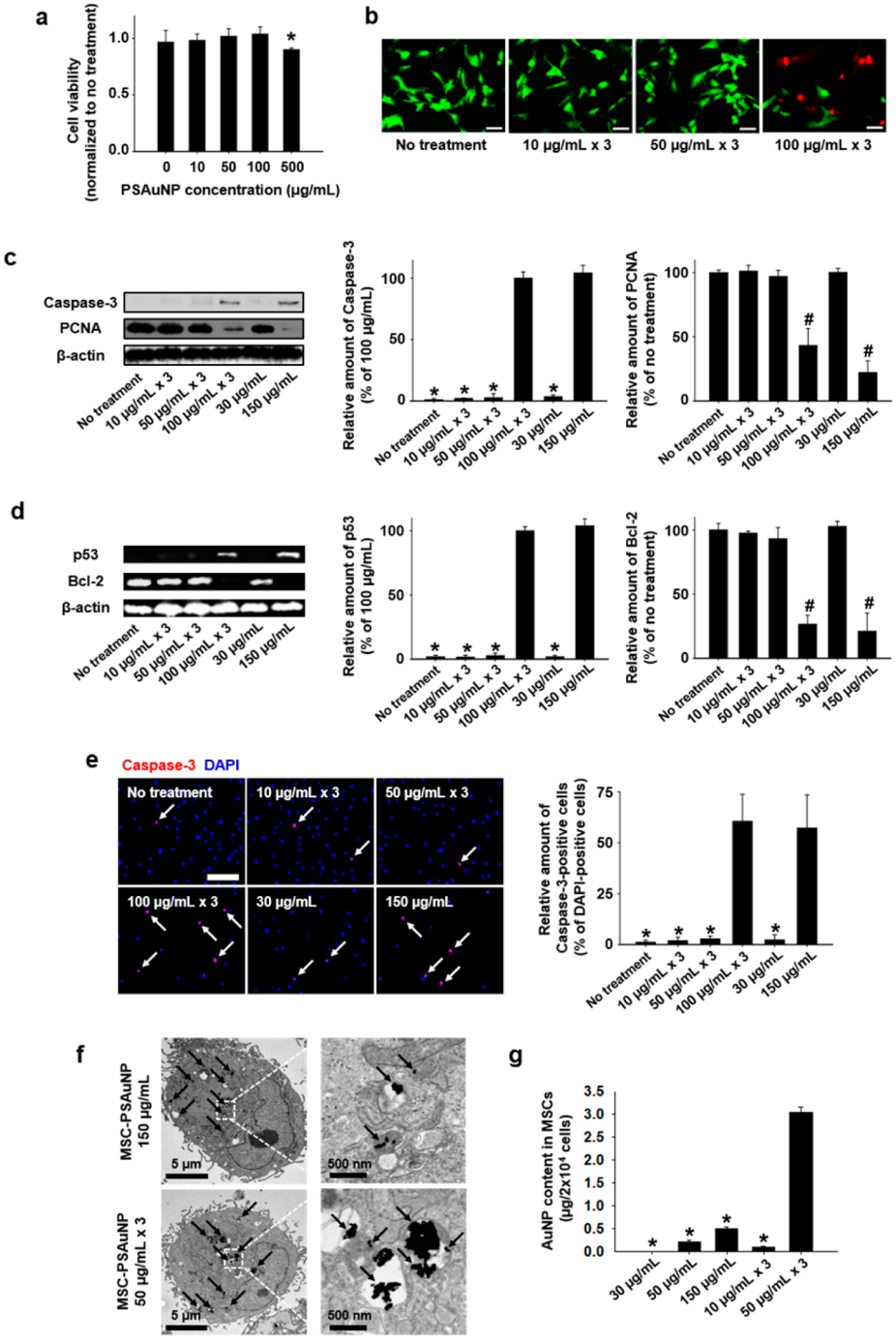

Figure 3. PSAuNP dose optimization and multiple treatments. Cytotoxicity of the PSAuNPs at various concentrations, which was evaluated by determining the viability of the MSCs according to (a) cell counting kit-8 assay following culture for 1 day with various concentrations of PSAuNPs. *$p < 0.05$ *versus* any group. (b) Fluorescence images of the MSCs stained with FDA/EB after three treatments with various concentrations of PSAuNPs. Green and red indicate viable and dead cells, respectively. Scale bars = 100 μm. (c) Apoptotic and proliferation activity of the MSCs after one or three treatments with various concentrations of PSAuNPs, as evaluated *via* Western blotting for a pro-apoptotic marker (caspase-3) and a cell proliferating marker (PCNA). *$p < 0.05$ *versus* the 100 μg/mL $\times$ 3 or the 150 μg/mL group. $^{\#}p < 0.05$ *versus* the no-treatment group. The apoptotic activity of the MSCs after one or three treatments with various concentrations of PSAuNPs, as evaluated (d) *via* qRT-PCR for a pro-apoptotic marker (p53) and an anti-apoptotic marker (Bcl-2) or (e) *via* immunocytochemical staining for caspase-3 (red). The cell nuclei are stained with DAPI (blue). Scale bars = 100 μm. *$p < 0.05$ *versus* the 100 μg/mL $\times$ 3 or the 150 μg/mL group. $^{\#}p < 0.05$ *versus* the no-treatment group. (f) TEM images showing the intracellular localization of PSAuNPs in the MSCs after a single treatment with 150 μg/mL PSAuNPs or three consecutive treatments with 50 μg/mL PSAuNPs. The magnified images show the representative PSAuNP aggregates. (g) Intracellular amounts of PSAuNPs in the MSCs after a single treatment or three consecutive treatments with various concentrations of PSAuNPs, as evaluated *via* ICP-AES ($n = 4$). *$p < 0.05$ *versus* the 50 μg/mL $\times$ 3 group.

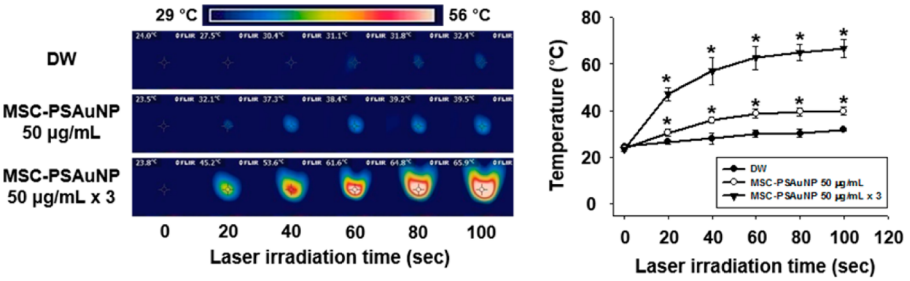

Figure 4. Photothermal effects of a single treatment and three consecutive treatments of MSCs with PSAuNPs. Temperatures were measured during laser irradiation (n = 5). *p < 0.05 *versus* any other group. DW indicates distilled water.

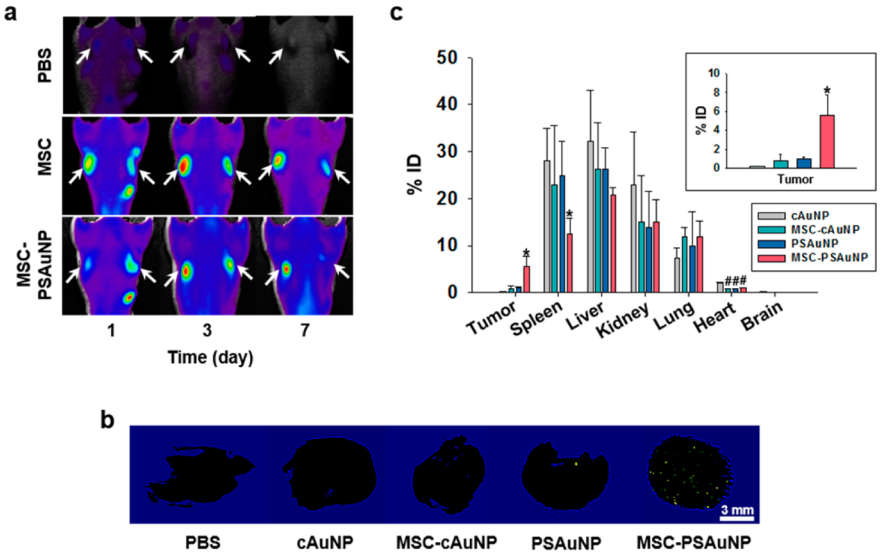

Figure 5. *In vivo* tumor-targeting and biodistributions of the AuNPs. (a) *In vivo* distribution of MSCs and MSC-PSAuNPs at various time points following intravenous injection into tumor-bearing mice. (b) Accumulation of AuNPs in the tumor 3 days after the intravenous injection, as evaluated *via* micro-CT imaging. Yellow indicates the AuNPs in the tumor. Scale bar = 3 mm. (c) Biodistributions of the AuNPs in the tumor tissues and major organs 3 days after intravenous injection of cAuNPs, MSC-cAuNPs, PSAuNPs, or MSC-PSAuNPs into tumor-bearing mice, as evaluated *via* ICP-AES (n = 3). *p < 0.05 *versus* any other group. $^{\#}p$ < 0.05 *versus* the cAuNP group.

restricted,[28] the endocytosis efficiency is limited. Therefore, the cells treated with a low concentration of nanoparticles for a longer time period internalize more nanoparticles than those treated with a high concentration of nanoparticles for a short time period.

***In Vitro* Photothermal Capability.** We next compared the photothermal effects of a single treatment and multiple treatments of MSCs with PSAuNPs by measuring the temperature rise after laser irradiation (660 nm, 0.5 W/cm^2) (Figure 4). The MSCs treated with a single dose of 50 μg/mL PSAuNPs exhibited a temperature increase of 16 °C, after 100 s of irradiation. Interestingly, the MSCs treated with 50 μg/mL PSAuNP × 3 exhibited a rapid temperature increase of 43 °C. This result demonstrated that the MSC treatments with PSAuNPs three times significantly enhanced the photothermal capability compared to the single treatment, which is attributed to the increased intracellular loading of PSAuNPs due to the multiple treatments.

***In Vivo* Tumor-Targeting Effect and Biodistributions of MSC-PSAuNPs.** We next investigated the tumor-targeting efficiency and the biodistributions of the MSC-PSAuNPs after intravenous administration to tumor-bearing mice. Tumors were generated *via* subcutaneous injection of human fibrosarcoma cell line (HT-1080 cells) to both flanks of athymic mice. After the tumors reached a proper volume, MSCs labeled with fluorescence were intravenously injected through the tail vein. First, the biodistributions of MSCs and MSC-PSAuNPs in the tumor-bearing mice were examined using a real-time live imaging system at 1, 3, and 7 days postinjection (Figure 5a). No signal was detected in the phosphate-buffered saline (PBS) injection control group. In contrast, the MSC and MSC-PSAuNP injection groups showed clear fluorescent signals and exhibited similar distribution patterns. At 1 day postinjection, the fluorescent signals were detected in both tumor and normal tissues. The signals were strongly detected only in tumor regions at 3 days postinjection and slightly decreased at 7 days postinjection. This result indicated that the number of MSCs or PSAuNP-laden MSCs in the tumor tissues reached a peak at 3 days postinjection. Furthermore, the tumor-tropic properties of MSCs were maintained even after MSCs were loaded with PSAuNPs.

Previous studies have demonstrated that MSCs preferentially migrate to tumor regions regardless of the tumor type.[29−31] The tumor tropism of MSCs involves interactions between the chemokines released from tumor tissues and the chemokine receptors expressed on the surfaces of MSCs. Tumor-secreted factors enhance the expression of CXC and CC receptors and activate growth factor receptors or toll-like receptors of MSCs.[32−36] MSCs then become more sensitized to chemoattractants, including CCL2,[32] CXCL8,[33] RANTES (CCL5),[34] PDGF-bb,[35] IGF-1,[34] and VEGF,[36] which are released from tumor tissues. These interactions between MSCs and tumor tissues increase the tumor-targeting efficiency of AuNPs in MSC-mediated AuNP delivery systems.

Next, to qualitatively investigate the *in vivo* tumor-targeting efficiency, the AuNPs in tumor tissues were imaged using micro-CT at 3 days after intravenous injection of either PBS, cAuNPs, MSC-cAuNPs, PSAuNPs, or MSC-PSAuNPs (Figure 5b). The micro-CT analysis showed that the injection of MSC-PSAuNPs resulted in the accumulation of a higher amount of AuNPs in the tumor tissues compared to the other groups. Furthermore, the MSC-PSAuNP group showed an even distribution of AuNPs within the tumor tissues. The improved intratumoral distribution of AuNPs facilitates a uniform temperature increase throughout the tumor tissues and consequently enhances the efficacy of photothermal cancer therapy.[17]

To investigate the biodistributions of the MSC-PSAuNPs following intravenous injection into tumor-bearing mice, the amount of AuNPs localized in the tumor tissues and major organs (spleen, liver, kidney, lung, heart, and brain) was determined using ICP-AES at 3 days postinjection (Figure 5c). All of the groups exhibited large amounts of AuNPs accumulated in the reticuloendothelial (spleen, liver, and lung) and urinary (kidney) systems, which is in accordance with the results of a previous study.[26] For the AuNP accumulation in the tumors, the MSC-PSAuNP group showed the highest tumor-targeting efficiency of 5.6 ± 2.1% ID (injected dose), which was 37-fold higher than that of the cAuNP group. The tumor-targeting efficiency of AuNPs in our MSC-PSAuNP system is even higher than that of a previous study (2−3% ID) in which AuNPs were decorated with a tumor-targeting moiety (transferrin).[37] Furthermore, the tumor-targeting efficiency of the MSC-PSAuNP group was 6.8-fold and 5.7-fold higher than the MSC-cAuNP group and the PSAuNP group, respectively. This result indicates that the tumor-targeting efficiency of AuNPs can be maximized when PSAuNPs and MSCs are applied together. The highest tumor-targeting efficiency of MSC-PSAuNPs is likely attributed to the tumor-tropic properties of MSCs and the prevention of AuNP exocytosis *via* forming PSAuNP aggregates. Taken together, the MSC-PSAuNP system significantly enhanced the tumor-targeting efficiency of AuNPs.

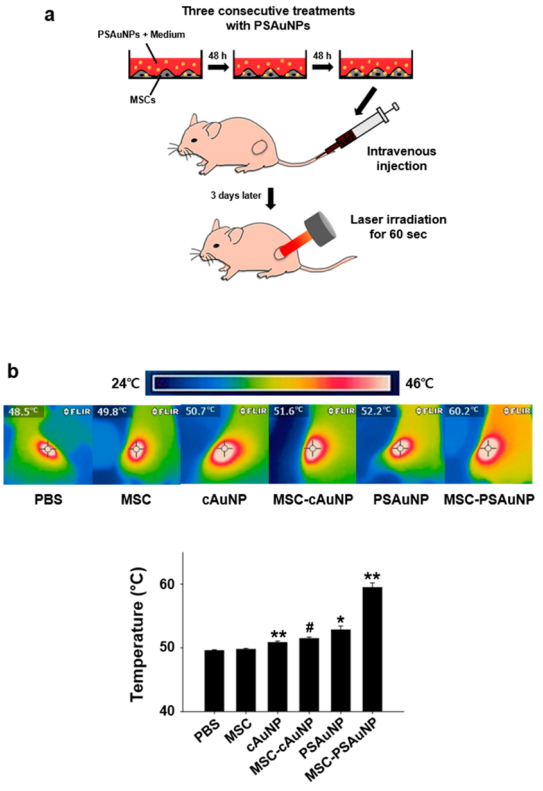

Figure 6. *In vivo* photothermal efficiency. (a) Schematic illustration of photothermal cancer therapy using the MSC-PSAuNPs. The MSCs were treated three times with 50 μg/mL PSAuNPs for 2 days each and then intravenously injected into tumor-bearing mice. After 3 days, the tumors were exposed to NIR laser light for 60 s under anesthesia. (b) Real-time infrared thermal images and temperature increases at the tumor sites after irradiation for 60 s (n = 4). **p < 0.05 *versus* any other group, *p < 0.05 *versus* any other group except the MSC-cAuNP group, $^{\#}p$ < 0.05 *versus* any other group except the PSAuNP group.

***In Vivo* Photothermal Efficiency.** The photothermal efficiency of the MSC-PSAuNPs was examined in a tumor-bearing mouse model. As shown in Figure 6a, MSCs were treated with medium containing 50 μg/mL PSAuNPs or cAuNPs three times for 2 days each. After the tumor reached a diameter of 7 mm, the PSAuNP-laden MSCs were injected intravenously. As controls, PBS, cAuNPs, MSC-cAuNPs, or PSAuNPs were also injected. At 3 days postinjection, the tumors were irradiated with a 660 nm laser at a power density of 0.5 W/cm^2 for 60 s. Since the real-time infrared thermal imaging system measures the skin temperatures only, the temperatures in the tumor tissues would be higher than the recorded values. As shown in Figure 6b, the MSC-PSAuNP group exhibited the largest temperature increase of 23.3 °C. This result is likely attributed to the improved tumor-targeting efficiency and photothermal effect of AuNPs *via* tumor tropism of MSCs, formation of the AuNP aggregates in MSCs, and prevention of AuNP exocytosis. Although laser irradiation in the PBS, MSC, cAuNP, and MSC-cAuNP groups induced comparable temperature increases of 13.4−15.3 °C,

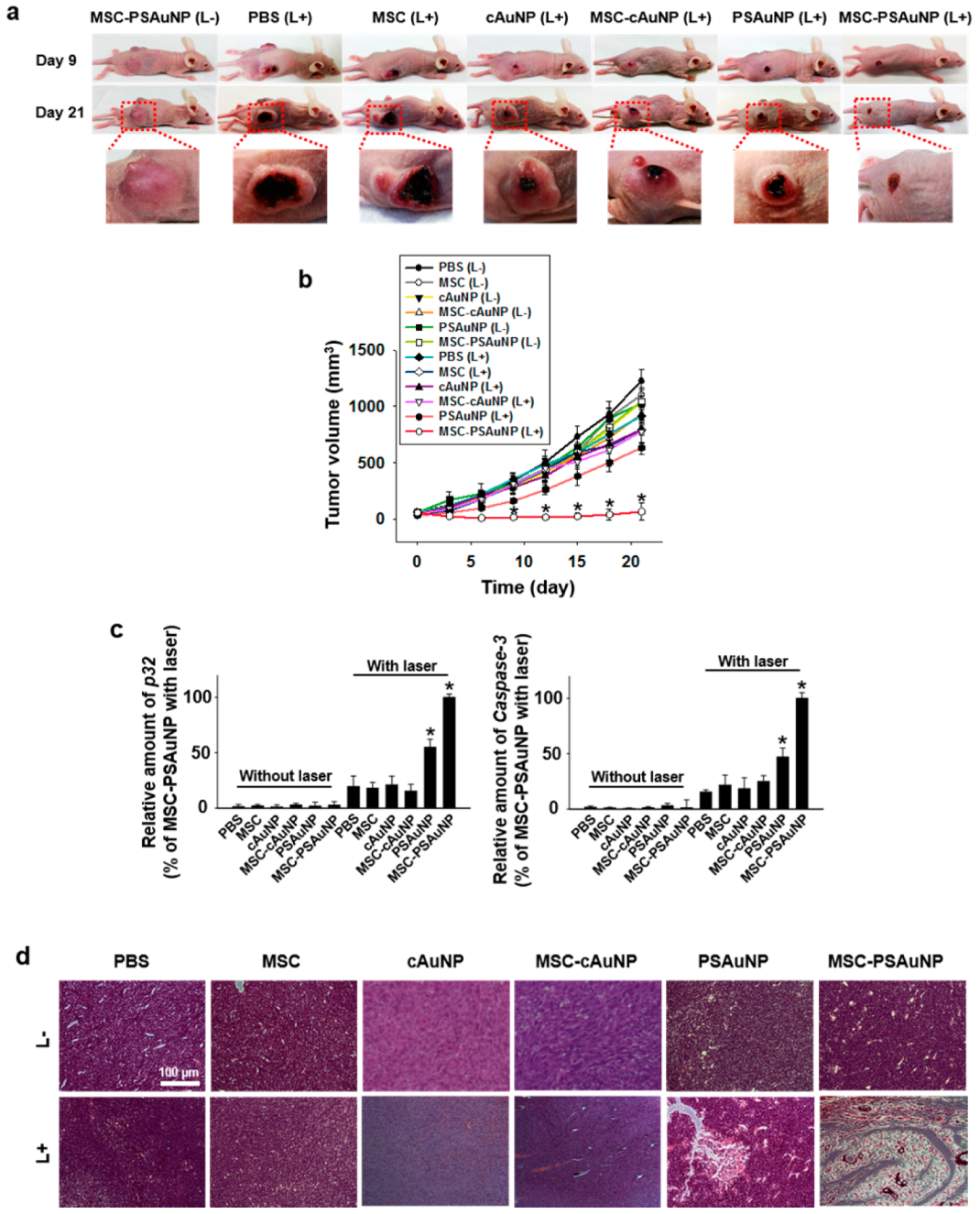

Figure 7. ***In vivo*** **photothermal therapeutic effects. (a) Representative images of the laser irradiation groups and MSC-PSAuNP (L−) group at day 9 and 21. Magnified images indicate the tumor regions. L+ refers to laser irradiation, and L− refers to no laser irradiation. (b) Volume profiles of each tumor tissue over 21 days after laser irradiation ($n = 8$). *$p < 0.05$** ***versus*** **any other group. (c) Apoptotic activity in the tumor tissues at day 9, as evaluated** ***via*** **qRT-PCR analysis for p32 and caspase-3 ($n = 4$). *$p < 0.05$** ***versus*** **any other group. (d) Hematoxylin and eosin staining images of thin sections of the tumor tissues with or without irradiation at day 21. Scale bar = 100 μm.**

the PSAuNP group showed a larger temperature increase of 17.0 °C (Figure 6b). This result is likely attributed to the larger size of the PSAuNP aggregates compared to the cAuNP.

In Vivo **Photothermal Cancer Therapy.** We next evaluated the *in vivo* anticancer therapeutic efficacy of the MSC-PSAuNPs. The tumor-bearing mice were randomly divided into 12 groups according to the intravenously injected material type (PBS, MSC, cAuNP, MSC-cAuNP, PSAuNP, or MSC-PSAuNP) with or without laser irradiation. At 3 days postinjection, a selection of the mice were exposed to laser irradiation (660 nm, 0.5 W/cm^2) for 60 s, and all of the mice were observed for 21 days (Figure 7a, Supporting Information Figure S3). The mice in the MSC-PSAuNP (L+) group exhibited scabs in the tumor region (Figure 7a) and an imperceptible tumor size at day 9 (Figure 7b). At day 21, no signs of tumor tissues were observed in most of the mice (Figure 7b).

Compared to the MSC-PSAuNP (L+) group, the other irradiation groups showed 9.4- to 13.7-fold larger tumor volumes at day 21 (Figure 7b).

There is a controversy about the function of MSCs in tumor growth.[38] Previous studies have demonstrated that MSCs exhibited an antitumor effect by inhibiting angiogenesis[39] and inducing apoptosis of tumor cells in a cell-number-dependent manner.[40] In contrast, the pro-tumor effect of MSCs was demonstrated in other studies.[41,42] MSCs promoted proliferation and metastasis of tumor cells in osteosarcoma[41] and colon carcinoma models.[42] In our study, the MSC (L−) group showed comparable tumor growth to the PBS (L−) group (Figure 7b), which indicated that MSCs did not affect the tumor growth.

To understand the pathological mechanisms of the photothermal therapy of the MSC-PSAuNPs, the mRNA expression levels of p32 and caspase-3 in the tumor tissues were examined using qRT-PCR. The gene expressions of p32 and caspase-3 are induced by thermal stress[43] and apoptosis signaling,[44] respectively. As shown in Figure 7c, only the laser irradiation groups exhibited perceptible levels of p32 mRNA expression. The MSC-PSAuNP (L+) group showed the greatest upregulated expression of p32 compared to the other laser irradiation groups. Furthermore, the mRNA expression levels of caspase-3 were similar to those of p32 (Figure 7c). The MSC-PSAuNP (L+) group exhibited the highest expression of caspase-3. These results demonstrated that MSC-PSAuNP (L+) induced the most fatal thermal stress, which promoted apoptosis signaling in the tumor tissues. Histological analysis of the tumor tissues indicated that the PSAuNP (L+) and MSC-PSAuNP (L+) groups exhibited partial and nearly complete destruction of the tumor cells, respectively (Figure 7d). In the other group, cytotoxic damage was not observed. Meanwhile, photothermal cancer therapy may not cause tumor cell dispersion that encourages metastatic tumor repopulation at distal sites, as a previous study reported that photothermal therapy slightly inhibited metastatic tumor growth by releasing tumor-associated antigens and inducing immunological responses.[45]

CONCLUSIONS

In this study, we demonstrate that the tumor-targeting efficiency and photothermal effect of AuNP-mediated anticancer therapy can be greatly improved by employing PSAuNPs and MSCs. PSAuNPs loaded into MSCs cluster together likely in acidic endosomes. We show that PSAuNP-laden MSCs delivered AuNPs at a high efficiency (5.6% ID) to targeted tumor tissues due to the tumor-tropic properties of MSCs and the prevention of the exocytosis of large PSAuNP aggregates. The high tumor-targeting efficiency and the large PSAuNP aggregates led to a dramatically enhanced photothermal efficiency and increased anticancer therapeutic efficacy upon NIR laser irradiation on tumor-bearing mice. This material- and cell-based anticancer therapy may be used in the future for successful cancer treatments.

METHODS

Cell Culture. Human MSCs (hMSCs) and the human fibrosarcoma cell line (HT-1080) were purchased from Lonza (USA) and American Type Culture Collection (ATCC; USA), respectively. MSCs and HT-1080 cells were cultured in Dulbecco's modified Eagle's medium (Gibco BRL, USA) supplemented with 10% (v/v) fetal bovine serum (Gibco BRL) and 1% (v/v) penicillin/streptomycin (Gibco BRL). The cells are incubated at 37 °C with 5% CO_2 saturation. The medium was changed every 2 days. After four passages, the hMSCs were used for experiments.

Synthesis and Characterization of cAuNPs and PSAuNPs. To synthesize the cAuNPs, 5 mL of a 60 nM 10 nm-sized citrate AuNP solution was adjusted to pH 10.5 using a 1 M NaOH aqueous solution (Sigma-Aldrich, USA), and a 100 mM 11-mercaptoundecanoic acid (MUA) solution (300 μL, 30 μmol, Sigma-Aldrich) in methanol was added. The mixture was stirred at room temperature for 19 h and centrifuged at 1400*g* for 5 min to remove the excess solid MUA. The reaction solution was dialyzed using Amicon ultracentrifugal filters (100 kDa Mw cutoff) for purification. To prepare the PSAuNPs, 4-(2-(6,8-dimercaptooctanamido)ethylamino)-3-methyl-4-oxobut-2-enoic acid (pH-sensitive ligand) was synthesized as previously described.[9] (±)-α-Lipoic acid (2.00 g, 9.70 mmol, Sigma-Aldrich) was dissolved in 12 mL of anhydrous chloroform. Then, 1,1-carbonyldiimidazole (2.00 g, 12.3 mmol, Sigma-Aldrich) was added to the lipoic acid solution, and the solution was stirred for 5 min at room temperature. The resultant solution was added into ethylenediamine (3.5 mL, 48.4 mmol) and stirred for 40 min in an ice bath and for another 30 min at room temperature. The crude product was washed three times with 10% (w/v) NaCl aqueous solution and once with water. It was dried with sodium sulfate, and the solvent was removed using a rotary evaporator to obtain *N*-(2-aminoethyl)-5-(1,2-dithiolan-3-yl)pentanamide. Citraconic anhydride (0. 68 mL, 7.5 mmol) was added dropwise into 15 mL of an anhydrous chloroform solution of *N*-(2-aminoethyl)-5-(1,2-dithiolan-3-yl)pentanamide (5.0 mmol). The solution was stirred overnight at room temperature. The precipitate was filtered and washed with anhydrous chloroform. The synthesized product (0.26 g, 0.72 mmol) was dissolved in 5 mL of water, and the pH was adjusted to 10 using a 2 M NaOH aqueous solution. An equal molar amount of sodium borohydride was added to the solution and stirred at room temperature for 30 min. Then, the pH-sensitive ligands were eventually obtained and directly used for surface exchange of the 10 nm-sized, citrate-capped AuNPs that were synthesized *via* the conventional Turkevich method.[46] After 10 h, the reaction solution was dialyzed using the Amicon ultracentrifugal filters (100 kDa Mw cutoff) three times for purification.

The UV−vis absorption spectra were obtained using an Agilent 8453 UV−vis spectrophotometer (Agilent Technologies). TEM images were obtained using a JEM-2100 (JEOL Ltd.). Surface charges and hydrodynamic sizes were measured using a Zetasizer Nano Z and a Zetasizer Nano S (Malvern Instruments Ltd.), respectively.

Intracellular Distributions of AuNPs. The MSCs were cultured on a 150 mm dish (1×10^6 cells/well) and incubated with 100 μg/mL cAuNPs or PSAuNPs for 24 h. The cells were then fixed using Karnovsky's fixative for 4 h at 4 °C and rinsed three times with cold 0.05 M cacodylate buffer. The cells were fixed with 1% osmium tetraoxide for 2 h at 4 °C and washed twice with cold distilled water. The samples were treated with 0.5% uranyl

acetate overnight at 4 °C, dehydrated using graded concentrations of ethanol (30, 50, 70, 80, 90, 95, and 100%), rinsed with propylene oxide, and finally embedded in Spurr's resin, which were then polymerized at 70 °C for 24 h. Thin sections with thicknesses of 100 nm were obtained using an ultramicrotome (Leica), collected on 200-mesh copper grids, and observed using a TEM (JEM-1010, JEOL Ltd.).

Quantification of Gold Amount Using ICP-AES. The MSCs were incubated with 100 μg/mL of cAuNPs or PSAuNPs for 24 h, rinsed with PBS three times, and collected *via* trypsinization. The suspended cells were lysed with aqua regia, and the gold amount was determined *via* ICP-AES (Thermo Electron Co.).[26] In this analysis, we set the control as the AuNP content in wells without cells, which were treated with the medium containing cAuNPs or PSAuNPs and then washed with PBS three times. The control values were subtracted from the gold amounts of the experimental groups.

AuNP Exocytosis Analysis. The hMSCs (2×10^4 cells/well) were incubated with 100 μg/mL cAuNPs or PSAuNPs for 24 h, rinsed with PBS three times, and cultured in fresh medium. At various time points, the cells were washed and collected *via* trypsinization. The amount of gold remaining in the MSCs at various time points was determined *via* ICP-AES. The fraction of exocytosed AuNPs (F_{exo}) was calculated using the equation $F_{exo} = (N_0 - N_t)/N_0$, where N_0 is the amount of gold before exocytosis at $t = 0$ and N_t is the gold amount remaining in the cells at each time point.[20]

Laser Irradiation and Photothermal Imaging. To evaluate the *in vitro* photothermal effect of the AuNPs, the MSCs were cultured on six-well plates (1×10^5 cells/well) and incubated with cAuNP 90 μg/mL, PSAuNP 30 μg/mL, or PSAuNP 90 μg/mL for 24 h. After rinsing three times with PBS, MSC-cAuNPs or MSC-PSAuNPs were collected *via* trypsinization and suspended in 20 μL of distilled water (DW). The samples (1×10^5 cells in 20 μL of DW) loaded in 200 μL microcentrifuge tubes were then irradiated using a 660 nm CW laser beam for 100 s at a power density of 0.5 W/cm^2. The temperature variations and photothermal images of the AuNP-laden MSCs during laser irradiation were recorded every 20 s using an infrared thermal imaging system (FLIR i2, FLIR Systems Inc.).

Cytotoxicity Analyses of the PSAuNPs. Cell viability was evaluated using a CCK-8 (Dojindo Molecular Technologies, Inc.). The CCK-8 assay measures the amount of formazan dye that is reduced by the intracellular dehydrogenase activities.[47] The number of living cells is proportional to the amount of the formazan dye. Briefly, the MSCs (1×10^4 cells/well) were cultured on 24-well plates with various concentrations of PSAuNPs for 24 h and rinsed with PBS three times. After replenishing the wells with fresh medium, CCK-8 solution was added into each well and incubated for 2 h. Then, the absorbance was measured at 450 nm using a plate reader. The cell viability was calculated as the percentage of viable cells relative to the AuNP-untreated cells ($n = 5$ per group).

Apoptotic and Proliferation Activities of the MSCs. The MSCs were cultured on six-well plates (1×10^5 cells/well) for 1 day and treated with various concentrations of PSAuNPs three times for 2 days' incubation for each. The live and dead cells were detected using fluorescein diacetate (FDA, 5 mg/mL) and ethidium bromide (EB, 10 mg/mL), respectively. The MSCs treated with the PSAuNPs at various concentrations three times were incubated in FDA/EB solution for 5 min at 37 °C and rinsed with PBS. The stained cells were examined using a fluorescence microscope. The apoptotic and proliferation activities of the cells treated with the PSAuNPs at various concentrations were evaluated *via* Western blot analysis and RT-PCR analysis. The Western blot analysis was performed to determine the protein expression of proliferation and pro-apoptotic (caspase-3) markers. The samples were centrifuged at 4 °C (15000*g*, 10 min) and resuspended in a cold lysis buffer (50 mM Tris-HCl, pH 8.0, 150 mM NaCl, 1% Nonidet P-40) containing a protease inhibitor cocktail for 40 min. Protein extracts were then centrifuged at 4 °C (14 000 rpm, 20 min). The protein concentration was determined using a bicinchoninic acid protein assay (Pierce Biotechnology). The protein extracts were loaded onto a 10% (w/v) SDS-PAGE, and the gels were transferred to a nitrocellulose membrane using an iBLOT system (Invitrogen). The membrane was blocked with 5% milk in Tris-buffered saline with Tween 20 (TBST) at room temperature for 1 h and then incubated with the primary antibody at room temperature for 1 h. The membrane was washed five times for 10 min each and then incubated with either horseradish peroxidase-conjugated anti-mouse or -rabbit antibody in TBST for 30 min. The immunoreactivity was visualized using enhanced chemiluminescence ($n = 3$ per group).The mRNA expression of pro-apoptotic (p53) and anti-apoptotic (Bcl-2) markers was evaluated using RT-PCR. Thirty-five cycles of PCR were performed, consisting of denaturating (94 °C, 30 s), annealing (60 °C, 30 s), extension (72 °C, 45 s), and a final extension at 72 °C for 7 min. The PCR products were visualized *via* electrophoresis on 1.5% (w/v) agarose gels with EB staining. The gels were read using a gel documentation system (GL 2200 PRO Imaging system; Carestream). The primer sequences used are shown in Table 1. The apoptotic activity of the cells was also evaluated using immunocytochemical staining with antibodies against caspase-3 (Abcam, UK). The immunoreactivity was visualized using rhodamine-conjugated secondary antibodies (Jackson Immuno Research Laboratories Inc., West Grove, PA, USA). The samples were counterstained with 4′,6-diamidino-2-phenylindole (DAPI, Vector Lbt.) and imaged using a fluorescence microscope (IX71 inverted microscope, Olympus).

TABLE 1. Primer Sequences Analyzed for the Quantification of β-Actin, Caspase-3, PCNA, p53, Bcl-2, and p32 Gene Expression Levels

gene	primer
β-actin	sense 5′-TGA GAC CTT CAA CAC CCC AGC-3′
	antisense 5′-GAT GTC ACG CAC GAT TTC CCT-3′
caspase-3	sense 5′-TTA ATA AAG GTA TCC ATG GAG AAC ACT-3′
	antisense 5′- TTA GTG ATA AAA ATA GAG TTC TTT TGT GAG-3′
PCNA	sense 5′-GCC GAG ATC TCA GCC ATA TT-3′
	antisense 5′-ATG TAC TTA GAG GTA CAA AT-3′
p53	sense 5′-CGG GAT CCA TGG AGG AGC CGC ACT CAG AT-3′
	antisense 5′-CCG CTC GAG TTT CTG GGA AGG GAC AGA AGA-3′
Bcl-2	sense 5′-ACC GTC GTG ACT TCG CAG AG-3′
	antisense 5′-GGT GTG CAG ATG CCG GTT CA-3′
p32	sense 5′-ACA GGG GCA GAA GGC TGA AGA-3′
	antisense 5′-GGT CCG CAA GGA AAT CCA TTA-3′

Intracellular Loading of the PSAuNPs and *in Vitro* Photothermal Effect *via* Multiple Treatments of the MSCs with PSAuNPs. After the MSCs were treated either with PSAuNP 50 μg/mL three times or with a single treatment of PSAuNP 150 μg/mL, the intracellular loading of the PSAuNPs was examined using TEM, as previously described. To quantify the amount of AuNPs loaded into the MSCs, the MSCs were incubated with a single treatment of 30, 50, or 150 μg/mL PSAuNPs or with three consecutive treatments of 10 or 50 μg/mL PSAuNPs. The intracellular AuNP amount was then quantified *via* ICP-AES. To evaluate the *in vitro* photothermal effect, the MSCs were incubated with a single treatment of 50 μg/mL PSAuNPs or with three consecutive treatments of 50 μg/mL PSAuNPs. After rinsing three times with PBS, the MSC-PSAuNPs were collected *via* trypsinization and irradiated using a 660 nm laser for 100 s. The temperature and photothermal images of the MSC-PSAuNPs were recorded every 20 s using an infrared thermal imaging system.

***In Vivo* MSC Imaging.** *In vivo* experiments were conducted using six-week-old female BABL/c athymic nude mice (Orient Bio, Seoul, Korea). The mice were anesthetized with xylazine (10 mg/kg) and ketamine (100 mg/kg), and the HT-1080 human fibrosarcoma cells (5×10^6 cells in 100 μL) were subcutaneously injected into both flanks of the mice. The mice were randomly sorted for treatments when the tumors reached approximately 7 mm in diameter, as measured using a digital caliper. For treatments, the mice were anesthetized, and MSCs or MSC-PSAuNPs (1×10^6 cells in 100 μL) that were labeled with VivoTrack 680 and suspended in 100 μL of PBS were intravenously injected *via* the tail vein ($n = 3$ animals). After 1, 3, and 7 days, the biodistributions of MSCs or MSC-PSAuNPs in the

tumor-bearing mice were examined using an eXplore Optix System (Advanced Research Technologies Inc.). The animal study was approved by the Institutional Animal Care and Use Committee of Seoul National University (SNU-140513-6-1).

Biodistribution of the AuNPs in the Tumors and Major Tissues. The MSCs (3×10^5 cells) were incubated with the same concentration (50 μg/mL) of PSAuNPs or cAuNPS for 2 days, and the AuNP incubation process was repeated three times. The MSC-PSAuNPs or MSC-cAuNPs were rinsed with PBS, suspended in PBS solution, and injected intravenously into the tumor-bearing mice when the tumors reached approximately 7 mm in diameter. Each mouse in the MSC-cAuNP group and MSC-PSAuNP group received 1×10^6 cells and 2×10^6 cells, respectively, since these numbers of cells contained the same amount (153 μg) of AuNPs (Supporting Information Figure S4). PBS, cAuNP, or PSAuNP solutions were also intravenously administered as control groups. The cAuNP, MSC-cAuNP, PSAuNP, and MSC-PSAuNP groups received the same amount (153 μg) of AuNPs per mouse. The gold amount of each group was determined *via* ICP-AES prior to the intravenous administration. For the CT analysis, the tumor tissues were fixed in 4% paraformaldehyde in PBS for 24 h at 3 days postintravenous injection. The CT images of the tumor tissues were obtained using a micro-CT system (SkyScan-1076; Skyscan, 40 kV, 250 mA) and CT image processing was performed using CT analyzer software (Skyscan). To quantify the amount of AuNPs in the tumor tissues and major organs (spleen, liver, kidney, lung, heart, and brain), the mice were sacrificed at 3 days postintravenous injection, and the tissues and organs were retrieved and lysed using aqua regia. The amount of AuNPs in the tissues and organs was determined *via* ICP-AES and expressed as a percentage of the injected dose of AuNPs.

***In Vivo* Photothermal Cancer Therapy.** When the tumors reached approximately 7 mm in diameter, PBS, cAuNPs, MSC-cAuNPs (2×10^6 cells), PSAuNPs, or MSC-PSAuNPs (1×10^6 cells) in 100 μL of PBS were intravenously injected into each of the tumor-bearing mice. Each mouse of the cAuNP, MSC-cAuNP, PSAuNP, and MSC-PSAuNP groups received the same amount (153 μg) of AuNPs. After 3 days postinjection, the tumor tissues were exposed to a laser (660 nm CW diode laser, *ca.* 1 cm diameter, 0.5 W/cm^2) for 60 s with anesthesia or not. The temperature variations at the tumor regions were recorded using a real-time infrared thermal imaging system (FLIR i2). The tumor sizes were measured at regular intervals using a digital caliper. The tumor volume was estimated according to the ellipsoidal calculation, $V = a \times b^2 \times 0.5$, where a is the largest and b is the smallest diameter.[26] qRT-PCR was performed to determine the relative mRNA expression levels of pro-apoptotic markers, p32 and caspase-3, in the tumor cells after 9 days postlaser irradiation. qRT-PCR reactions were performed using a Step One Plus real-time PCR system (Applied Biosystems) with TOPreal qPCR 2X PreMIX (Enzynomics). Each cycle consisted of the following temperatures: 94 °C for 3 s and 60 °C for 30 s. The primer sequences used are shown in Table 1. For the histological analysis, the tumor tissues were retrieved at 21 days postlaser irradiation and fixed in 4% paraformaldehyde in PBS. The samples were embedded in paraffin and sectioned at a thickness of 6 μm. The sections of the tumor tissues were stained using hematoxylin and eosin and examined using an optical microscope.

Statistical Analysis. Quantitative data were expressed as the means ± standard deviations. The statistical analysis was performed using one-way analysis of variance (ANOVA) with Tukey's significant difference *post hoc* test using SPSS software (SPSS Inc., USA). A value of $p < 0.05$ was considered to denote statistical significance.

Conflict of Interest: The authors declare no competing financial interest.

Acknowledgment. This research was supported by the National Research Foundation of Korea (2014073757) and the Korea Health Industry Development Institute (KHIDI), Ministry of Health and Welfare (HI14C1550, HI14C3270, and HI15C0498), Republic of Korea.

Supporting Information Available: The Supporting Information is available free of charge on the ACS Publications website at DOI: 10.1021/acsnano.5b02207.

Figures S1−S4 (PDF)

REFERENCES AND NOTES

1. Zhang, Z.; Wang, J.; Chen, C. Near-Infrared Light-Mediated Nanoplatforms for Cancer Thermo-Chemotherapy and Optical Imaging. *Adv. Mater.* **2013**, *25*, 3869–3880.
2. Weissleder, R. A Clearer Vision for *In Vivo* Imaging. *Nat. Biotechnol.* **2001**, *19*, 316–317.
3. Sapareto, S. A.; Dewey, W. C. Thermal Dose Determination in Cancer Therapy. *Int. J. Radiat. Oncol., Biol., Phys.* **1984**, *10*, 787–800.
4. Jaque, D.; Martinez Maestro, L.; del Rosal, B.; Haro-Gonzalez, P.; Benayas, A.; Plaza, J. L.; Martin Rodriguez, E.; Garcia Sole, J. Nanoparticles for Photothermal Therapies. *Nanoscale* **2014**, *6*, 9494–9530.
5. Hildebrandt, B.; Wust, P.; Ahlers, O.; Dieing, A.; Sreenivasa, G.; Kerner, T.; Felix, R.; Riess, H. The Cellular and Molecular Basis of Hyperthermia. *Crit. Rev. Oncol. Hematol.* **2002**, *43*, 33–56.
6. Burke, A. R.; Singh, R. N.; Carroll, D. L.; Wood, J. C.; D'Agostino, R. B., Jr.; Ajayan, P. M.; Torti, F. M.; Torti, S. V. The Resistance of Breast Cancer Stem Cells to Conventional Hyperthermia and Their Sensitivity to Nanoparticle-Mediated Photothermal Therapy. *Biomaterials* **2012**, *33*, 2961–2970.
7. Choi, J.; Yang, J.; Jang, E.; Suh, J.-S.; Huh, Y.-M.; Lee, K.; Haam, S. Gold Nanostructures as Photothermal Therapy Agent for Cancer. *Anti-Cancer Agents Med. Chem.* **2011**, *11*, 953–964.
8. Huang, X.; Neretina, S.; El-Sayed, M. A. Gold Nanorods: From Synthesis and Properties to Biological and Biomedical Applications. *Adv. Mater.* **2009**, *21*, 4880–4910.
9. Nam, J.; Won, N.; Jin, H.; Chung, H.; Kim, S. pH-Induced Aggregation of Gold Nanoparticles for Photothermal Cancer Therapy. *J. Am. Chem. Soc.* **2009**, *131*, 13639–13645.
10. Gobin, A. M.; Lee, M. H.; Halas, N. J.; James, W. D.; Drezek, R. A.; West, J. L. Near-Infrared Resonant Nanoshells for Combined Optical Imaging and Photothermal Cancer Therapy. *Nano Lett.* **2007**, *7*, 1929–1934.
11. von Maltzahn, G.; Park, J. H.; Agrawal, A.; Bandaru, N. K.; Das, S. K.; Sailor, M. J.; Bhatia, S. N. Computationally Guided Photothermal Tumor Therapy Using Long-Circulating Gold Nanorod Antennas. *Cancer Res.* **2009**, *69*, 3892–3900.
12. Ayala-Orozco, C.; Urban, C.; Knight, M. W.; Urban, A. S.; Neumann, O.; Bishnoi, S. W.; Mukherjee, S.; Goodman, A. M.; Charron, H.; Mitchell, T.; *et al*. Au Nanomatryoshkas as Efficient Near-Infrared Photothermal Transducers for Cancer Treatment: Benchmarking against Nanoshells. *ACS Nano* **2014**, *8*, 6372–6381.
13. Hiramatsu, H.; Osterloh, F. E. A Simple Large-Scale Synthesis of Nearly Monodisperse Gold and Silver Nanoparticles with Adjustable Sizes and with Exchangeable Surfactants. *Chem. Mater.* **2004**, *16*, 2509–2511.
14. Choi, M. R.; Stanton-Maxey, K. J.; Stanley, J. K.; Levin, C. S.; Bardhan, R.; Akin, D.; Badve, S.; Sturgis, J.; Robinson, J. P.; Bashir, R.; *et al*. A Cellular Trojan Horse for Delivery of Therapeutic Nanoparticles into Tumors. *Nano Lett.* **2007**, *7*, 3759–3765.
15. Madsen, S. J.; Baek, S. K.; Makkouk, A. R.; Krasieva, T.; Hirschberg, H. Macrophages as Cell-Based Delivery Systems for Nanoshells in Photothermal Therapy. *Ann. Biomed. Eng.* **2012**, *40*, 507–515.
16. Choi, M. R.; Bardhan, R.; Stanton-Maxey, K. J.; Badve, S.; Nakshatri, H.; Stantz, K. M.; Cao, N.; Halas, N. J.; Clare, S. E. Delivery of Nanoparticles to Brain Metastases of Breast Cancer Using a Cellular Trojan Horse. *Cancer Nanotechnol.* **2012**, *3*, 47–54.
17. Mooney, R.; Roma, L.; Zhao, D.; Van Haute, D.; Garcia, E.; Kim, S. U.; Annala, A. J.; Aboody, K. S.; Berlin, J. M. Neural Stem Cell-Mediated Intratumoral Delivery of Gold

Nanorods Improves Photothermal Therapy. *ACS Nano* **2014**, *8*, 12450–12460.
18. Porada, C. D.; Almeida-Porada, G. Mesenchymal Stem Cells as Therapeutics and Vehicles for Gene and Drug Delivery. *Adv. Drug Delivery Rev.* **2010**, *62*, 1156–1166.
19. Devine, S. M.; Bartholomew, A. M.; Mahmud, N.; Nelson, M.; Patil, S.; Hardy, W.; Sturgeon, C.; Hewett, T.; Chung, T.; Stock, W.; *et al.* Mesenchymal Stem Cells Are Capable of Homing to the Bone Marrow of Non-Human Primates Following Systemic Infusion. *Exp. Hematol.* **2001**, *29*, 244–255.
20. Chithrani, B. D.; Chan, W. C. Elucidating the Mechanism of Cellular Uptake and Removal of Protein-Coated Gold Nanoparticles of Different Sizes and Shapes. *Nano Lett.* **2007**, *7*, 1542–1550.
21. Chithrani, B. D.; Ghazani, A. A.; Chan, W. C. W. Determining the Size and Shape Dependence of Gold Nanoparticle Uptake into Mammalian Cells. *Nano Lett.* **2006**, *6*, 662–668.
22. Jain, P. K.; Lee, K. S.; El-Sayed, I. H.; El-Sayed, M. A. Calculated Absorption and Scattering Properties of Gold Nanoparticles of Different Size, Shape, and Composition: Applications in Biological Imaging and Biomedicine. *J. Phys. Chem. B* **2006**, *110*, 7238–7248.
23. Huang, X.; Jain, P. K.; El-Sayed, I. H.; El-Sayed, M. A. Plasmonic Photothermal Therapy (PPTT) Using Gold Nanoparticles. *Lasers Med. Sci.* **2008**, *23*, 217–228.
24. Govorov, A. O.; Richardson, H. H. Generating Heat with Metal Nanoparticles. *Nano Today* **2007**, *2*, 30–38.
25. Schaeublin, N. M.; Braydich-Stolle, L. K.; Schrand, A. M.; Miller, J. M.; Hutchison, J.; Schlager, J. J.; Hussain, S. M. Surface Charge of Gold Nanoparticles Mediates Mechanism of Toxicity. *Nanoscale* **2011**, *3*, 410–420.
26. Nam, J.; La, W. G.; Hwang, S.; Ha, Y. S.; Park, N.; Won, N.; Jung, S.; Bhang, S. H.; Ma, Y. J.; Cho, Y. M.; et al. pH-Responsive Assembly of Gold Nanoparticles and "Spatiotemporally Concerted" Drug Release for Synergistic Cancer Therapy. *ACS Nano* **2013**, *7*, 3388–3402.
27. Wang, Y. C.; Black, K. C. L.; Luehmann, H.; Li, W. Y.; Zhang, Y.; Cai, X.; Wan, D. H.; Liu, S. Y.; Li, M.; Kim, P.; et al. Comparison Study of Gold Nanohexapods, Nanorods, and Nanocages for Photothermal Cancer Treatment. *ACS Nano* **2013**, *7*, 2068–2077.
28. Panariti, A.; Miserocchi, G.; Rivolta, I. The Effect of Nanoparticle Uptake on Cellular Behavior: Disrupting or Enabling Functions? *Nanotechnol., Sci. Appl.* **2012**, *5*, 87–100.
29. Kidd, S.; Spaeth, E.; Dembinski, J. L.; Dietrich, M.; Watson, K.; Klopp, A.; Battula, V. L.; Weil, M.; Andreeff, M.; Marini, F. C. Direct Evidence of Mesenchymal Stem Cell Tropism for Tumor and Wounding Microenvironments Using *In Vivo* Bioluminescent Imaging. *Stem Cells* **2009**, *27*, 2614–2623.
30. Studeny, M.; Marini, F. C.; Dembinski, J. L.; Zompetta, C.; Cabreira-Hansen, M.; Bekele, B. N.; Champlin, R. E.; Andreeff, M. Mesenchymal Stem Cells: Potential Precursors for Tumor Stroma and Targeted-Delivery Vehicles for Anticancer Agents. *J. Natl. Cancer Inst.* **2004**, *96*, 1593–1603.
31. Dwyer, R. M.; Kerin, M. J. Mesenchymal Stem Cells and Cancer: Tumor-Specific Delivery Vehicles or Therapeutic Targets? *Hum. Gene Ther.* **2010**, *21*, 1506–1512.
32. Dwyer, R. M.; Potter-Beirne, S. M.; Harrington, K. A.; Lowery, A. J.; Hennessy, E.; Murphy, J. M.; Barry, F. P.; O'Brien, T.; Kerin, M. J. Monocyte Chemotactic Protein-1 Secreted by Primary Breast Tumors Stimulates Migration of Mesenchymal Stem Cells. *Clin. Cancer Res.* **2007**, *13*, 5020–5027.
33. Ringe, J.; Strassburg, S.; Neumann, K.; Endres, M.; Notter, M.; Burmester, G. R.; Kaps, C.; Sittinger, M. Towards *In Situ* Tissue Repair: Human Mesenchymal Stem Cells Express Chemokine Receptors CXCR1, CXCR2 and CCR2, and Migrate upon Stimulation with CXCL8 but Not CCL2. *J. Cell. Biochem.* **2007**, *101*, 135–146.
34. Ponte, A. L.; Marais, E.; Gallay, N.; Langonne, A.; Delorme, B.; Herault, O.; Charbord, P.; Domenech, J. The *In Vitro* Migration Capacity of Human Bone Marrow Mesenchymal Stem Cells: Comparison of Chemokine and Growth Factor Chemotactic Activities. *Stem Cells* **2007**, *25*, 1737–1745.
35. Fiedler, J.; Roderer, G.; Gunther, K. P.; Brenner, R. E. BMP-2, BMP-4, and PDGF-bb Stimulate Chemotactic Migration of Primary Human Mesenchymal Progenitor Cells. *J. Cell. Biochem.* **2002**, *87*, 305–312.
36. Ball, S. G.; Shuttleworth, C. A.; Kielty, C. M. Vascular Endothelial Growth Factor Can Signal through Platelet-Derived Growth Factor Receptors. *J. Cell Biol.* **2007**, *177*, 489–500.
37. Choi, C. H.; Alabi, C. A.; Webster, P.; Davis, M. E. Mechanism of Active Targeting in Solid Tumors with Transferrin-Containing Gold Nanoparticles. *Proc. Natl. Acad. Sci. U. S. A.* **2010**, *107*, 1235–1240.
38. Hong, I. S.; Lee, H. Y.; Kang, K. S. Mesenchymal Stem Cells and Cancer: Friends or Enemies? *Mutat. Res., Fundam. Mol. Mech. Mutagen.* **2014**, *768*, 98–106.
39. Ho, I. A. W.; Toh, H. C.; Ng, W. H.; Teo, Y. L.; Guo, C. M.; Hui, K. M.; Lam, P. Y. P. Human Bone Marrow-Derived Mesenchymal Stem Cells Suppress Human Glioma Growth through Inhibition of Angiogenesis. *Stem Cells* **2013**, *31*, 146–155.
40. Lu, Y. R.; Yuan, Y.; Wang, X. J.; Wei, L. L.; Chen, Y. N.; Cong, C.; Li, S. F.; Long, D.; Tan, W. D.; Mao, Y. Q.; et al. The Growth Inhibitory Effect of Mesenchymal Stem Cells on Tumor Cells *in Vitro* and *in Vivo*. *Cancer Biol. Ther.* **2008**, *7*, 245–251.
41. Xu, W. T.; Bian, Z. Y.; Fan, Q. M.; Li, G.; Tang, T. T. Human Mesenchymal Stem Cells (hMSCs) Target Osteosarcoma and Promote Its Growth and Pulmonary Metastasis. *Cancer Lett.* **2009**, *281*, 32–41.
42. Zhu, W.; Xu, W. R.; Jiang, R. Q.; Qian, H.; Chen, M.; Hu, J. B.; Cao, W. K.; Han, C. X.; Chen, Y. C. Mesenchymal Stem Cells Derived from Bone Marrow Favor Tumor Cell Growth *in Vivo*. *Exp. Mol. Pathol.* **2006**, *80*, 267–274.
43. Park, J. H.; von Maltzahn, G.; Xu, M. J.; Fogal, V.; Kotamraju, V. R.; Ruoslahti, E.; Bhatia, S. N.; Sailor, M. J. Cooperative Nanomaterial System to Sensitize, Target, and Treat Tumors. *Proc. Natl. Acad. Sci. U. S. A.* **2010**, *107*, 981–986.
44. Porter, A. G.; Janicke, R. U. Emerging Roles of Caspase-3 in Apoptosis. *Cell Death Diff.* **1999**, *6*, 99–104.
45. Wang, C.; Xu, L. G.; Liang, C.; Xiang, J.; Peng, R.; Liu, Z. Immunological Responses Triggered by Photothermal Therapy with Carbon Nanotubes in Combination with Anti-CTLA-4 Therapy to Inhibit Cancer Metastasis. *Adv. Mater.* **2014**, *26*, 8154–8162.
46. Kimling, J.; Maier, M.; Okenve, B.; Kotaidis, V.; Ballot, H.; Plech, A. Turkevich Method for Gold Nanoparticle Synthesis Revisited. *J. Phys. Chem. B* **2006**, *110*, 15700–15707.
47. Ishiyama, M.; Miyazono, Y.; Sasamoto, K.; Ohkura, Y.; Ueno, K. A Highly Water-Soluble Disulfonated Tetrazolium Salt as a Chromogenic Indicator for NADH as Well as Cell Viability. *Talanta* **1997**, *44*, 1299–1305.